Exp. Theo. NANOTECHNOLOGY 10 (2026) 1501-1518 https://doi.org/10.56053/10.3.1501

Study the thermal shock resistance of Ni-WC composite nanostructure coating sprayed by thermal spray technique with different thickness

Alaa Zamel Dahesh[1,*], *Ahmed Mohammed Hassan*[1], *Hussain Mohammed Yousif*[2]

[1]Collage of Materials Engineering, University of Technology -Iraq, Baghdad, Iraq
[2]State Company for Steel Industries, Ministry of Industry and Minerals, Baghdad, Iraq
*) Email: mae.22.028@grad.uotechnology.edu.iq

Received 21/4/2026, *Received in revised form* 13/5/2026, *Accepted* 11/6/2026, *Published* 15/7/2026

In this study, a coating with a thickness of 200-300µm is applied to a nickel-based alloy using a thermal spray process. The top layer consisted of a tungsten carbide-reinforced nickel-based composite (WC), while the bond layer is made of a nickel-based superalloy. The Taguchi method, combined with the analysis of variance (ANOVA) used to determine the optimal coating conditions, which are achieved by selecting the following parameters: spray distance = 150 mm, transverse speed = 300 mm/min, and powder feeding rate = 30 g/min. This combination resulted in a low-porosity, high-adhesion nanostructure coating layer. The performance of the coating is evaluated through microhardness tests with a load of 9.8 N and thermal cycling tests. Samples are heated to 1100 °C in a furnace for 30 minutes, then rapidly cooled to room temperature with water. Additionally, results are analyzed using scanning electron microscopy (SEM) and X-ray diffraction (XRD). Findings indicated that the use of Ni-WC increased the hardness of coated samples by a factor of four compared to uncoated samples. Moreover, during the thermal cycling test, the thickness of the harmful thermal growth oxide (TGO) layer decreased by 51% as the coating thickness increased from 200µm to 300µm.

Keywords: Flame thermal spray (FTHS); Coating; Taguchi; Thermal cycles test; Turbine blades.

1. INTRODUCTION

The problem of damage to parts used in operating conditions at high temperatures exceeding 1000 °C is common. For example, in gas turbine engines, thermo- mechanical stresses are formed in the rotor blades in the high-pressure turbine (HPT) unit due to high pressure and high temperature [1]. Damages often occur at the leading or trailing edge or blade tip during service under severe operating conditions of pressure, heat, oxidation, and erosion, especially in dusty regions. Fig. 1 shows the most common defects diagnosed using a borescope during engine core (HPT) inspection [2]. Numerous studies have been conducted by researchers to select methods and materials with different designs that can endure severe operating conditions [3, 4]. Crucial materials used in aircraft engines, particularly for components such as turbine blades, discs, and other components in the hot core of the engine, are Ni alloys [5]. Their properties make them well-suited for the demanding conditions of aircraft engines, which include high operating temperatures, high rotational speeds, and all while enduring oxidizing and corrosive environments.

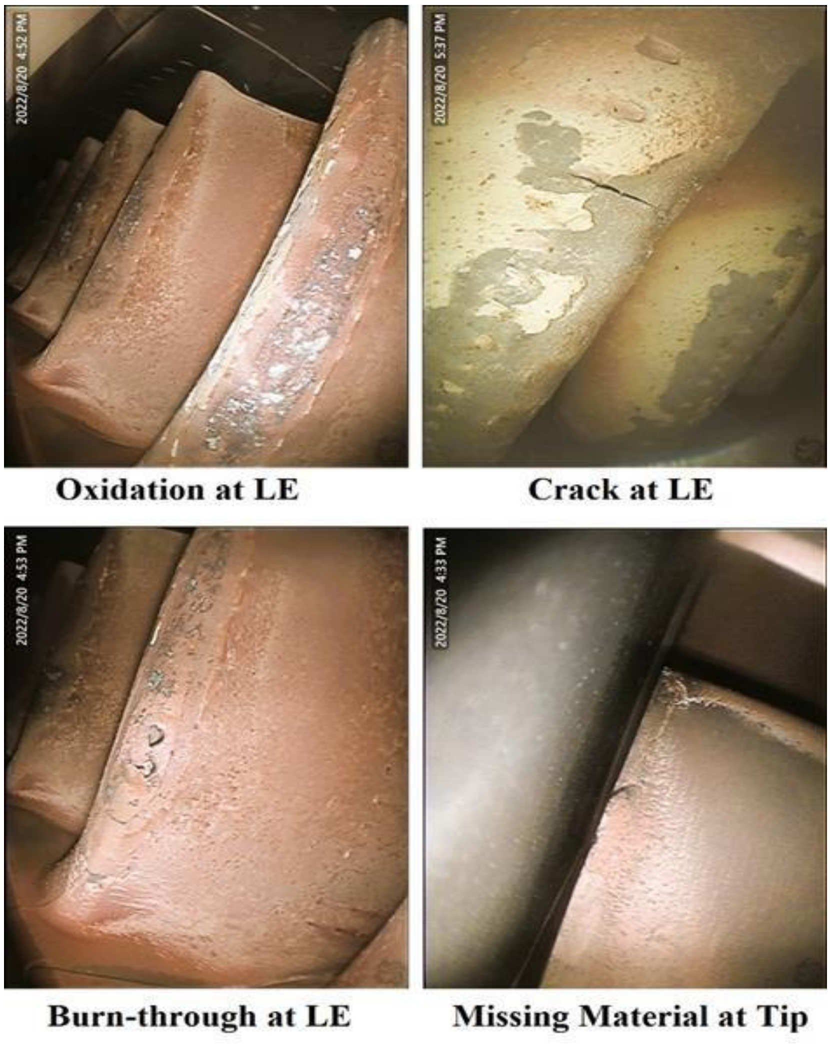

Figure 1 Defects of HPT-Bs.

These alloys contain a face-centered cubic (FCC) γ- Ni matrix that contains cohesive mineral precipitates, borides, carbides, and other phases, including gamma prime (γ′). Various elements are added to improve the performance of the alloy: chromium and aluminum enhance oxidation resistance; cobalt, molybdenum, and tungsten increase high-temperature toughness; and carbon boosts creep resistance. [6] One notable example of such an alloy is Inconel 718, which is widely used in the manufacture of turbine blades due to its exceptional thermo-mechanical properties. To further enhance the reliability and durability of nickel alloys in severe environments, a protective coating layer is typically applied to prevent damage to the blades. In high-temperature applications, coatings typically have a thickness of 100–500μm and are applied in two layers. The top layer (TC) can be made of ceramic materials, such as YSZ (yttria-stabilized zirconia), or composite materials that include nickel with reinforcements like WC (tungsten carbide) or Al_2O_3 (alumina). The bond layer (BC) is generally composed of metallic materials, such as NiCrAlY or NiCoCrAlY alloys. Ceramic nanomaterials are of great importance in the field of coatings due to their unique properties resulting from small particle size and increased surface area. [7,8] Choudhary et al. [9] have reported that although ceramic coating materials like YSZ exhibit excellent performance in harsh conditions, they often fail to match the substrate effectively due to differences in the coefficients of thermal expansion between the two layers. For instance, the coefficient of thermal expansion for nickel-based alloys is approximately 13×10^{-6}°C^{-1}. A promising solution to reduce the thermal expansion mismatch between the coating layers is to use metal matrix composite (MMC) coatings. For example, a nickel matrix reinforced with ceramic particles like WC can help achieve a better balance between thermal expansion and hardness. By increasing the reinforcement volume ratio, this approach improves the mismatch factor between the top layer and the bond layer, enhancing the adhesion between them. Furthermore, this reinforcement acts as a hard phase that boosts the erosion resistance of the coating [10, 11]. Coating layers can be applied via a variety of processes, including EB-PVD, laser, and thermal spraying methods such as HVOF, APS, and FTHS [12-14]. Among different coating methods along with some efficient assistant approaches such as Taguchi program [15, 16], and appropriate heat treatment (re-melting) [17, 18], the flame thermal spraying is considering a reliability and effectively technique for depositing coating have low porosity, free cracks [19] good resist to thermal shock, and effective wear/erosion protection [20] in economically way when compared with other costive and complicated coating techniques such as plasma spray and HVOF methods [21]. The major drawbacks of APS spraying are that the raw material injected radially into the plasma column is not sufficiently melted, which leads to the cooled droplets being deposited on the surface of the substrate [22]. In general, the porosity is inherently phenome in thermal sprayed coatings, including those deposited by HVOF, resulting in a limited-service life of the coating in the harsh environment [23]. In Flame Thermal Spray (FTHS), raw coating materials, whether in powder or wire form, are introduced into a combustion area, which can involve a flame, plasma, or electric arc, where they are melted. Following this, the air compressor is used to atomize the molten material through a nozzle towards the substrate surface, as illustrated in Fig. 2 [14, 24]. The adhesion and density of the deposited coating can be enhanced by designing appropriate experiments using Design of Experiments (DOE) methodologies. Many studies have successfully employed Taguchi's method as an optimization approach, which facilitates the production of high-quality coatings while minimizing the number of trials required [25,26].

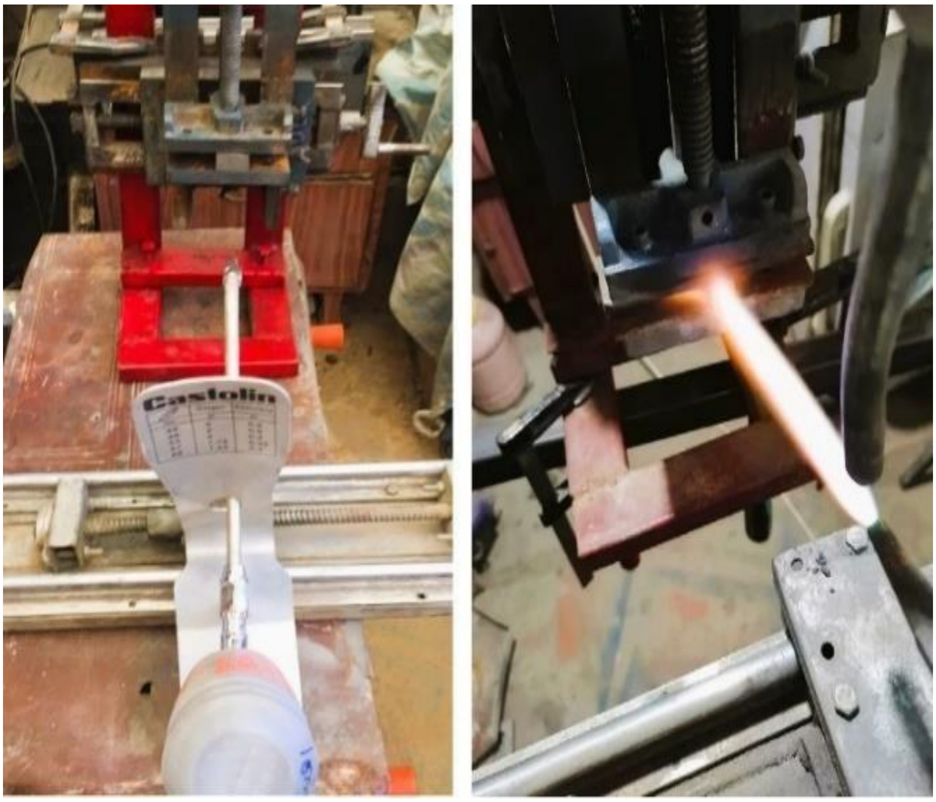

Figure 2 FTHS devise.

Rachida et al. [20] reported that the use of flame thermal spraying technology produced a low-porosity composite coating that is resistant to abrasion conditions due to the presence of carbide as the hard phase and tough alloy matrix. Fanicchia et al. [14] also achieved an 80% increase in thermal cycle life of the coating applied using FTHS technology compared to the APS process due to the coating's stress-tolerant performance. This study aims to verify the effectiveness of using nickel-based alloy (NiCrBSi) as a bond layer and a composite coating (Ni-WC) as a top layer, using the flame thermal spray technique, via nine runs, based on the Taguchi method. Microhardness and thermal shock tests are conducted on the sprayed coatings with varying thicknesses to assess their performance. Additionally, the results are analyzed using energy dispersive X-ray spectroscopy (EDS), scanning electron microscopy (SEM), and X-ray diffraction (XRD).

2. EXPERIMENTS AND PROCEDURE

2.1 Materials

The experimental specimens used in this study consist of flat specimens measuring 1cm x 1cm x 0.04cm and are made of IN718 material. To improve the surface roughness, the samples are scratched with fine silica. Following this, they are cleaned in an ultrasonic bath using isopropanol.
Two layers of coating are applied using a thermal spraying technique. The first layer, referred to as the bond layer, is composed of NiCrBSi powder (brand name 10009 Eutalloy, USA) with a particle size ranging from 20 to 97.2µm. The top coating layer consists of Ni- WC powder (brand name 10112

Eutalloy, USA) with a particle size ranging from 42.86 to 93.31μm. Table 1 presents the raw materials' chemical compositions used.

Table 1 Chemical composition (%) by weight of raw materials.

Materials	Nickel	Cr	B	Si	Al	Fe	C	Hf	W
IN-718 (substrate)	Base	17.1	0.5	0.3	0.5	18.5	0.07	-	-
NiCrBSi (BC)	Base	13.0	1.1	5.0	0.3	3.6	-	-	-
Ni-WC (TC)	Base	5.11	0.07	2.2	0.2	3.2	11.1	0.1	27

2.2 Flame thermal spray technique (FTHS) and Taguchi method

The coating layers are applied through flame thermal spraying, utilizing a gaseous mixture of oxygen at 0.5 bar and acetylene at 0.7 bar, with a SuperJet Eutalloy torch (SuperJet Eutalloy, Castoline Eutectics), as appears in Fig. 2. The uncoated and coated samples are illustrated in Fig. 3. Previous studies [18, 26] and tracking experiments indicate that producing coatings with high quality requires carefully designed experiments (DOE), which are structured using the Taguchi L9 (3^3) orthogonal matrix. The tests are conducted with varying standoff distances (SOD) (in mm), transverse speeds (TV) (in mm/min), and feed rates (FR) (in g/min), as detailed in Table 2.

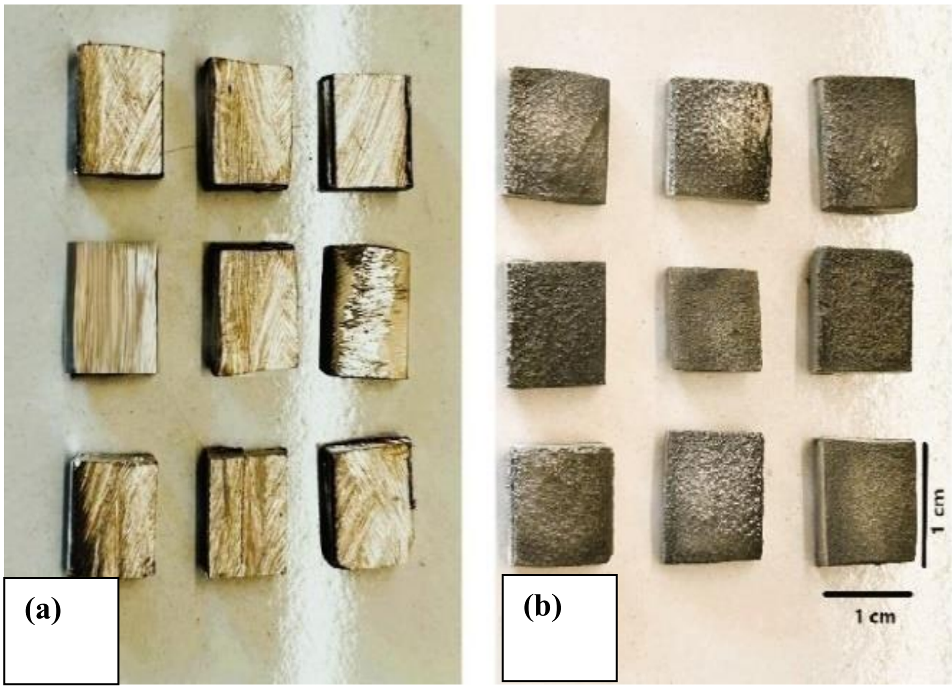

Figure 3 Specimens (a) uncoated, and (b) coated.

Table 2 Factors and levels of the Flame thermal spray technique

Parameter	Code	Level-1	Level-2	Level-3
SOD (Standoff distance) (mm)	A	100	125	150
TV (Traverse Velocity) (mm/min)	B	100	200	300
FR (Feed Rate) (g/min)	C	10	20	30

Prior research has determined that medium spray distances ranging from 100 to 150 mm are optimal for depositing high-quality, low-porosity coatings. A study by Mihoob et al. [27] demonstrated a decrease in adhesion strength when the standoff distance exceeded the intermediate range of 200 to 300 mm. Additionally, Mrdak R. et al. [28] found that using standoff distances below the medium range (80 to 120 mm) led to less effective layer formation.

2.3 Morphology and microstructural characterization

The depth of coating diffusion and thickness for 9 specimens are determined using optical microscopy. Photographs are taken at 40X magnification with Meiji Techno microscopes. A detailed examination of the phases and compositions of the raw materials and the coating is conducted using X-ray diffraction (XRD) with a Shimadzu diffractometer. The X-ray diffractograms are processed using Xpert HighScore Plus software from Panalytical Technologies Pvt. Ltd., the Netherlands [29]. The voltage and current settings are 40 kV and 100 mA, respectively, and the angle of diffraction (2θ) ranged from 20° to 80°. Additionally, a scanning electron microscope (SEM) equipped with energy-dispersive X-ray spectroscopy (EDX) is used to assess the morphology of the coating surface at various magnifications. This method also facilitated the investigation of the porous interfacial zone and the chemical composition of the coatings, employing a Thermo Scientific™ Axia ChemiSEM™.

2.4 Microhardness test

Three samples each of the coated and uncoated samples are used to test the hardness using a Vickers microhardness tester (HVS 1000 Digital). 9.8 N is the load used, and 15 seconds is the holding time. For each sample, three readings are determined, and the average of these readings represented the hardness value [30].

2.5 Thermal Shock Test

In the thermal cycling test conducted on coated samples with thicknesses of (200, 250, 300) μm, three flat samples measuring (1 × 1 × 0.4) cm are used. The samples are heated to 1100 °C in a furnace for 30 minutes, then rapidly cooled to room temperature with water over 10 seconds, as illustrated in Fig. 4. After cooling, the samples are dried. The test continued until signs of coating failure are observed, with more than 10% coating removal considered a failure criterion. The weights of the samples are measured before and after each cycle. To analyze and discuss the test results, surface and cross-sectional morphology examinations are performed using Scanning Electron Microscopy (SEM) and Energy Dispersive X-ray Spectroscopy (EDS) [1,31,32].

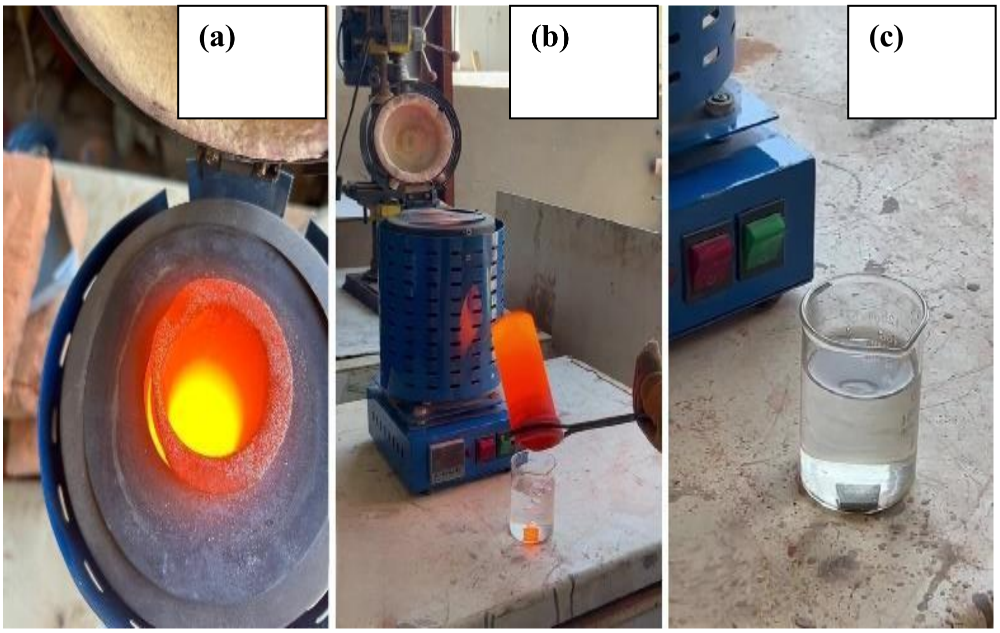

Figure 4 Thermal shock test: (a) heating at 1100 °C in a furnace, (b) taking out the specimen from the furnace after 30 minutes, (c) water cooling.

3. RESULTS AND DISCUSSION

3.1 Taguchi method

Nine testing operations are followed according to the proposed design according to the Taguchi method, and the results are tabulated in Table 3.

Where the depths of penetration in mm are Trial1, Trial2, and Trial3, and the S/N equation used in this research is the bigger is better as shown in eq. 1

$$S/N = -10 \, . \log_{10}\left(sum \, \frac{1}{Y^2}\right) n \quad (1)$$

Table 3 Results of Taguchi orthogonal matrix (OA).

Code	A	B	C	T1	T2	T3	Mean	S/N
1	100	100	10	51	53	48	50.66	34.0
2	100	200	20	66	64	61	63.66	36.0
3	100	300	30	67	69	67	67.66	36.6
4	125	100	20	47	48	44	46.33	33.3
5	125	200	30	55	53	54	54	34.6
6	125	300	10	64	58	60	60.66	35.6
7	150	100	30	72	71	72	71.66	37.1
8	150	200	10	66	68	65	66.33	36.4
9	150	300	20	59	56	61	58.66	35.3

T: Trial.

In this study, the response variable is denoted as Y (the depth of diffusion), and n represents the number of repetitions of the experiment, which is three. The results presented in Table 3 indicate that the greatest spread is achieved in round 7, characterized by SOD of 150 mm, TV of 100 mm/min, and FR of 30 g/min. To determine which parameters, require control to achieve coating with good properties, a response table of the signal-to-noise ratio (S/N) is utilized. The parameter with the largest difference in delta value, defined as the difference between the highest average S/N and the lowest average S/N for each parameter, exerts the most significant influence on the response. This is further illustrated in Table 4.

Table 4 Results of response of coating spread to parameters studied.

Level	A	B	C
1	35.59	34.84	35.4
2	34.54	35.72	34.92
3	36.3	35.88	36.12
Delta	1.76	1.04	1.2
Rank	1	3	2

The results indicate that SOD (A) had the highest delta value, 1.76, making it the parameter with the greatest influence on coating spread (ranked 1st). In contrast, TV (B) had the least influence among the other parameters, with a value of 1.04 (ranked 3rd), as shown in Table 4. Based on the data in Tables 3 and 4, Fig. 5 shows the main effect plot of the means, generated using Minitab 18.

Figure 5 Diffusion depth main effect plot for means.

The optimal coating conditions are achieved by selecting the following parameters: A3 (SOD = 150 mm), B3 (TV = 300 mm/min), and C3 (FR = 30 g/min). The diffusion depth increased over 10μm when the SOD is raised from 125 mm to 150 mm. Additionally, an increase in the FR from 20 g/min to 30 g/min resulted in an improvement of about 8μm in diffusion depth. Furthermore, the diffusion depth also increased over 6μm when the TV is increased from 100 mm/min to 300 mm/min. The analysis of variance (ANOVA), combined with the Taguchi method, is one of the most widely used statistical techniques for studying experimental results and determining the impact of each factor [30]. As illustrated in Table 5, the results based on the signal-to- noise ratio and ANOVA indicate that parameter A (SOD) has the greatest influence on the diffusion value, accounting for 37.64% of the effect. This is followed by parameter C (FR), which contributes 17.4%, and parameter B (TV) with 15.01%.

Table 5 ANOVA for S/N ratio.

Source	DF	Seq SS	Adj SS	Adj MS	F	P	Contribution, %
SOD (A)	2	4.71	4.71	2.35	1.26	0.44	37.64
TV (B)	2	1.87	1.87	0.93	0.5	0.66	15.01
FR (C)	2	2.18	2.18	1.09	.59	0.63	17.4
Residual error	2	3.73	3.73	1.86			29.85
Total	8	12.51					100

These findings suggest that the distance between the nozzle and the substrate, along with the powder feed rate, significantly affects both the temperature and speed of the sprayed coating. As a result, a larger portion of the dissolved coating powder is deposited onto the substrate, leading to fewer oxidation products. These results are consistent with those reported in other studies [34, 35]. Three confirmatory experiments are conducted to assess the response characteristics, specifically the depth of propagation, at the optimal levels of the process variables (A3, B3, C3). These experiments served as validation tests to confirm the results obtained earlier. Average experimental values are calculated and compared with the expected values. According to Table 6, the experimental results align closely with the expected outcomes, achieving a confidence level of 0.95 [36]. The results from Experiments 1, 2, and 3 yielded propagation efficiencies of 98.6%, 98.7%, and 99%, respectively, which are very close to the expected efficiencies determined using the optimization process by the Taguchi method.

Table 6 Confirmation experiments under optimal conditions.

Exp. No.	A	B	C	P. diffusion	Exp. Diffusion
1	3	3	3	72.4	71.43
2	3	3	3	72.4	72.01
3	3	3	3	72.4	72.39

3.1. Morphology and microstructure characterization

Figs. 6a and 6b display the coated samples along with their cross-sections, highlighting the shape and size of the diffusion zone. The typical coating layers consist of an interdiffusion zone (IDZ), a bond coat (BC), and a top coat (TC). The diffusion depth and resulting coating thickness are measured using an optical microscope at 40x magnification. The average total coating thickness ranged from 200 to 300μm.

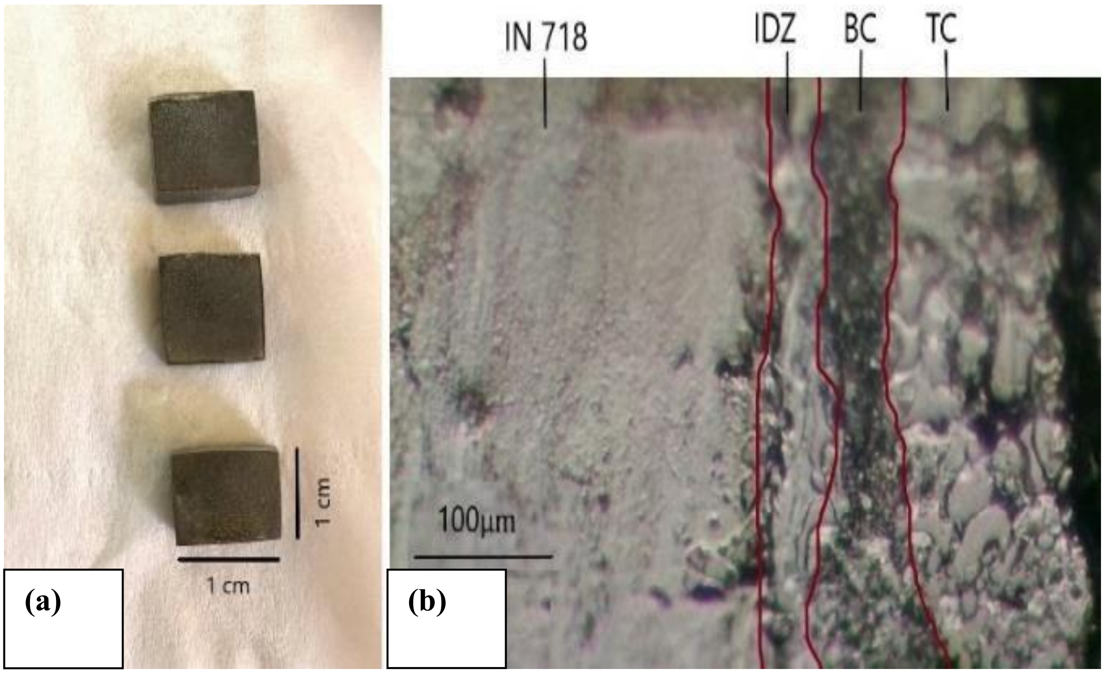

Figure 6 (a) Optimize Samples (b) diffusion depth of coating using optical microscopy.

The results from the scanning electron microscopy (SEM) and energy dispersive spectroscopy (EDS) are presented in Fig. 7. The surface and cross-section of the coated sample are depicted in Figs 7a and 7b. As observed, the coating layers are applied to the substrate continuously and uninterruptedly, without any microcracks at the interface. This success can be attributed to the optimal spraying conditions established following the Taguchi method. The coatings exhibit high density and a homogeneous microstructure, with spherical particles ranging in size from 300 nm to 1.6µm. This finding confirms the complete dissolution of most coating materials, which are deposited uniformly on the substrate with a porosity of less than 4%. The EDS results indicate the presence of all coating elements, as shown in Fig. 7c.

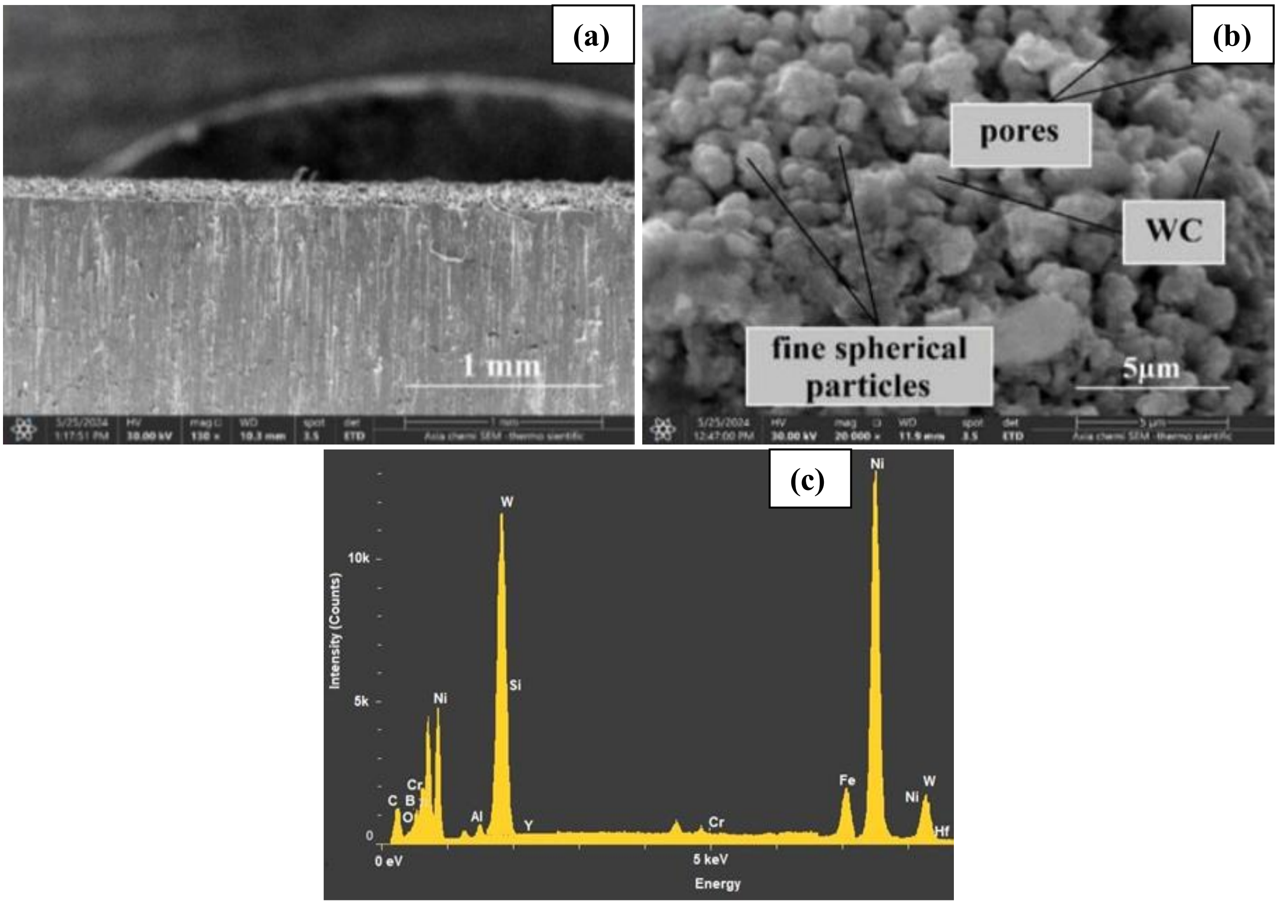

Figure 7 SEM images of coated samples: a) cross-section; b) coating surface; c) EDS results of coating layer.

The XRD patterns in Fig. 8a and b show that the coating consists essentially of the same phases detected in the raw material, but at a higher intensity and with good distribution on the substrate. This supports the SEM-EDS results for coating. A series of thermodynamic phase transitions occurred within the primary coating materials, as detailed in eq. (2-8) [37].

$$23Cr + 6C = Cr_{23}C_6 \quad (2)$$

$$7Cr + 3C = Cr_7C_3 \quad (3)$$

$$W + C = WC \quad (4)$$

$$2W + C = W_2C \quad (5)$$

$$3Ni + Si = Ni_3Si \quad (6)$$

$$3Ni + \mathrm{Al} = Ni_3\mathrm{Al} \quad (7)$$

$$Cr + B = CrB \quad (8)$$

This process resulted in the formation of a dense and homogeneous coating layer on the substrate [19]. The coating mainly features an amorphous structure, which is represented by a matrix solid solution of γ-Ni, alongside a crystallized structure that is stabilized by various metallic compounds. Notably, the coating contains significant quantities of carbide phases like WC and $Cr_{23}C_6$, smaller amounts of W_2C and Cr_7C_3, and borides such as CrB [38]. This combination results in a coating characterized by both crystalline and amorphous properties. The increase in carbides is attributed to the disintegration of some of the wettable WC at high temperatures, which results in the withdrawal of C from some elements that surround it. This WC and other carbides contribute to the higher hardness and wear resistance [39,40].

Additionally, intermetallic compounds like Ni_3Al, Ni_3Nb, and Ni_3Si contribute to increased strength and enhanced resistance to oxidation and creep of the nickel-based material at elevated temperatures [41, 42]. This is demonstrated by the results of hardness, thermal shock, and erosion tests that are introduced later in the results discussion section. Most of these results are common to NiCrBSi and Ni-WC coatings prepared by the different thermal deposition techniques (e.g., APS and HVOF) and laser coating [18,43].

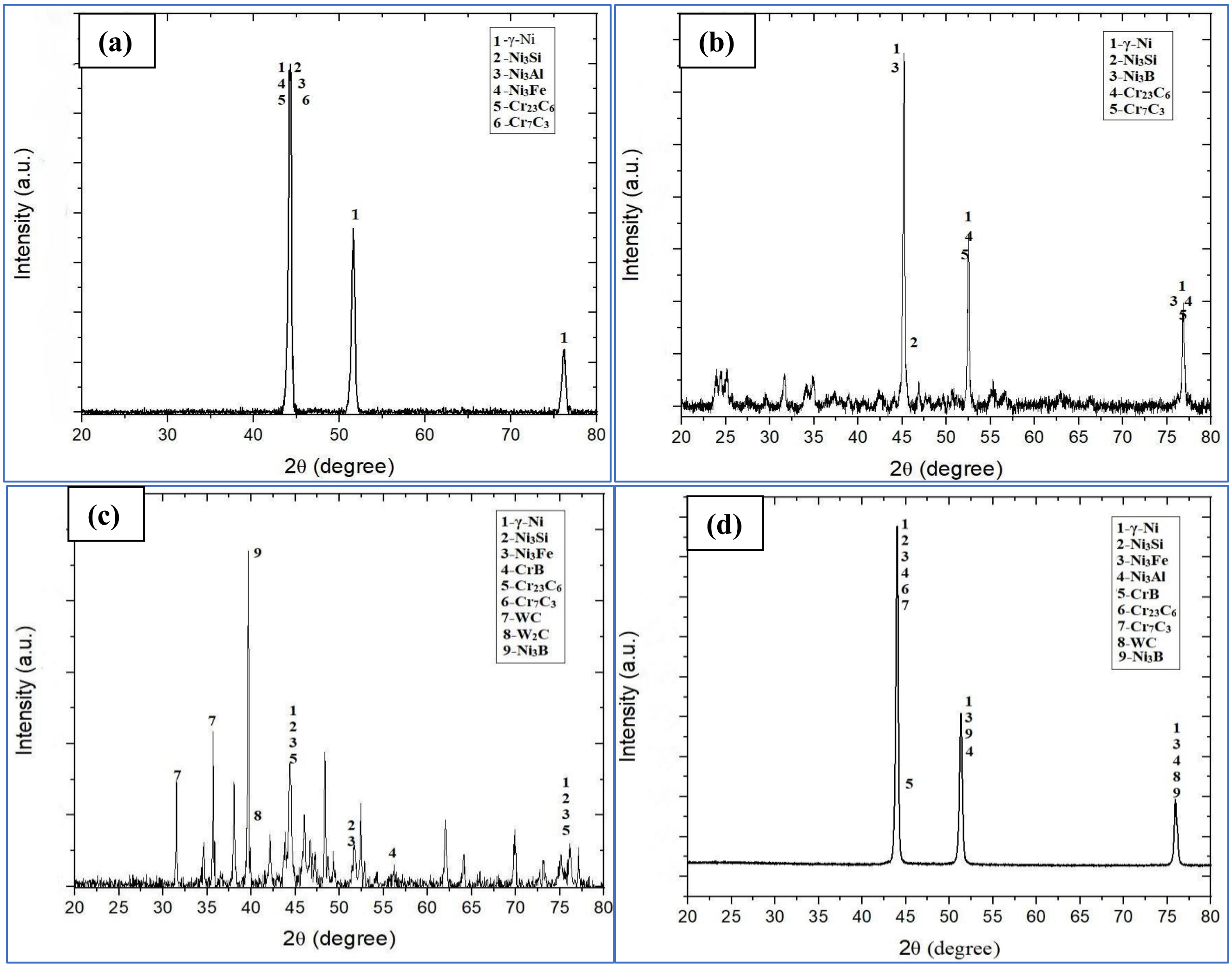

Figure 8 XRD patterns of: (a) substrate IN718, (b) BC (NiCrBSi) powder, (c) TC (Ni-WC) powder, (d) the coating layer.

3.2. Microhardness test

Microhardness testing is performed on both uncoated and coated specimens. The hardness of the uncoated specimen is measured at 210 HV, whereas the microhardness of the coated specimen reached

940 HV, as illustrated in Fig. 9. The increased microhardness of the coated sample can be attributed to the denser and more cohesive layer deposited on the substrate, which contains solid carbide phases, primarily tungsten carbide and borides, that are uniformly applied through the flame thermal spray process. This is supported by the results obtained from SEM-EDS and XRD analyses, conducted under optimized spraying parameters determined using Taguchi [18, 43].

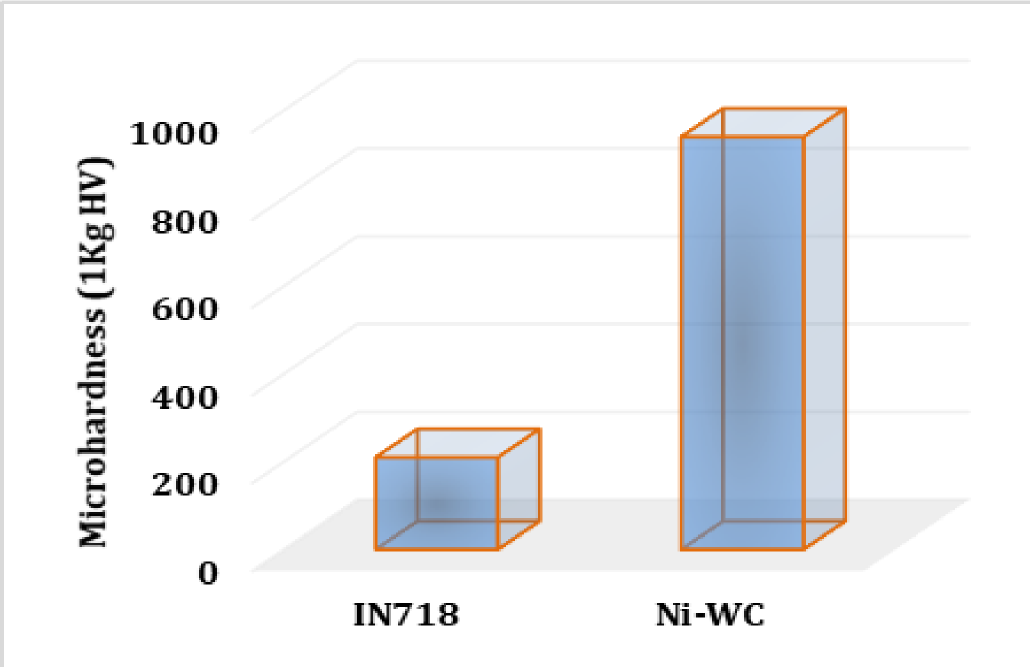

Figure 9 Micro-hardness test results of uncoated and coated samples.

3.3. Thermal shock test

Three samples are tested for each coating thickness. The thermal cycling results for these samples are depicted in Fig. 10. Similar to the findings reported by Shi et al. [44], Fig.s 10a to 10c illustrate a linear decrease in the weight of the samples as the number of cycles increases. In Fig. 10d, it is shown that, after 600 thermal cycles, the peeling off for the 300µm-thick sample is approximately 1%, for the 250µm thick sample it is 5%, and for the 200µm-thick sample it is 9.6%. The latter is close to the coating failure criterion of 10%. Based on previous studies, coating degradation and failure are attributed to a combination of factors. These include thermal stress resulting from the temperature gradient between the coating and the substrate, as well as the presence of thermally harmful oxides (TGO), which can lead to the formation and growth of thermal cracks at the interface between the bond coat and thermal barrier (BC/TC), ultimately resulting in coating peeling [45]. Fig. 10e shows that coating failure occurred at the specimen edges where stress is concentrated, a finding previously described by Pourbafrani et al. [46]. TGO thickness measurements are taken from 20 positions in the SEM images after 600 cycles. The results indicated that the rate of thermal growth oxide (TGO) layer formation decreased with increasing coating thickness, as illustrated in Fig. 11. The results presented in Fig. 12 demonstrate a 51% reduction in TGO thickness when the coating thickness increased from 200µm to 300µm. This conclusion is further supported by research conducted by Ashofteh et al. [47].

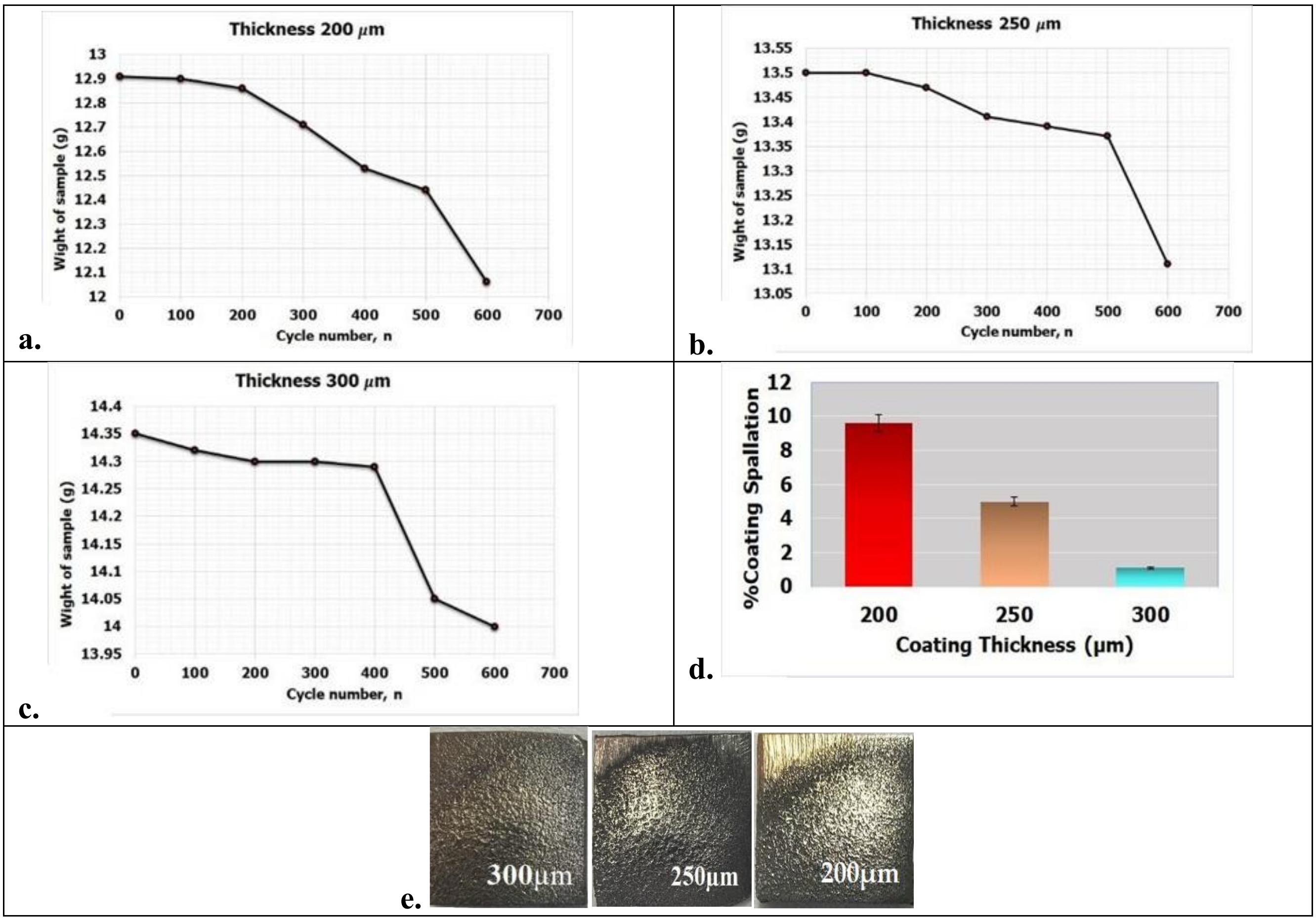

Figure 10 Thermal cycling test results: a-c) weight change as a function of cycle number for samples with different thickness coatings, d) thermal cycling lifetime, e) samples after 600 thermal cycles.

From Fig. 11(b, d, f), it is noted that the erosion effects are more pronounced in the edge region. This is attributed to the formation of detrimental thermal growth oxide layers (Al_2O_3 and spinel-like NiO) caused by the oxidation of the NiCrAlY layer at high temperatures. These layers contributed to the development of thermal stress at the BC/TC interface, resulting in fragmentation and failure of part of the top coating, as confirmed by the energy-dispersive spectroscopy (EDS) analysis results shown in Fig. 11(c, e, g) [1, 48]. The 300-μm-thick coating sample demonstrated the best thermal shock resistance. This improvement can be attributed to the use of Ni-WC as the top layer, which contains phases such as WC (27%), besides Ni_3Al, Ni_3Si, and Cr_7C_3. These components enhanced the coating's erosion resistance and minimized the formation of harmful oxide layers.

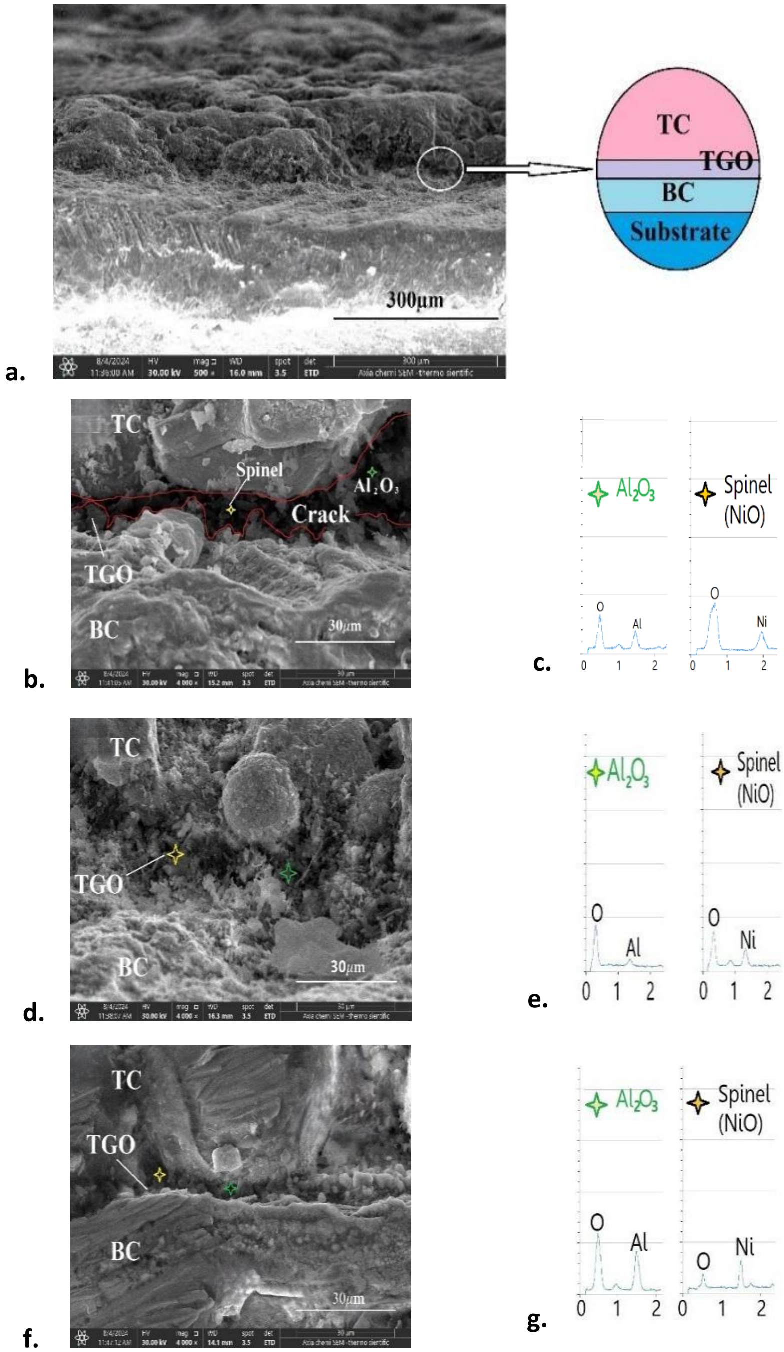

Figure 11 (a) SEM and schematic representation of the coating sample. (b-g) SEM and EDS of coating samples with different thicknesses in the edge region after 600 thermal cycles. (b) SEM for 200 µm, (c) EDS of 200 µm, (d) SEM for 250 µm, (e) EDS of 250 µm, (f) SEM for 300 µm, (g) EDS of 300 µm.

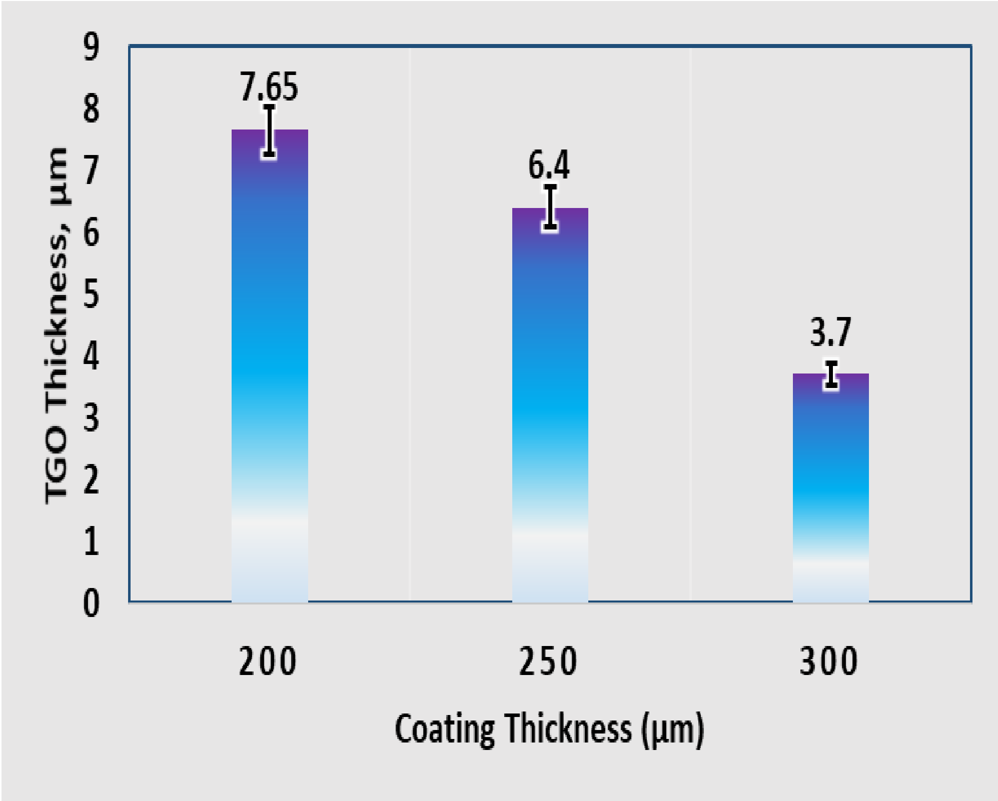

Figure 12 Thickness of TGO as a function of thermal cycles at 1100 °C after 600 cycles.

Table 7 presents the results of this study in comparison to previous research. In this work, the average thermal shock lifetime is approximately 600 cycles when using the optimized NiCrBSi (BC) and Ni-WC (TC) coating systems, with heating at 1100°C for 30 minutes per cycle. Poursaeidi et al. [1] reported that crack formation and growth occurred in the interlayer between BC and TC after about 120 cycles (heating at 1070°C for 3 minutes per cycle) when applying a ZrO2- 8wt% Y_2O_3 coating using the APS process. Pourbafrani et al. [46] found that the peeled area of their coating expanded by more than 20% after 450 cycles (heating at 1100°C for 10 minutes per cycle) when using a non-commercial coating material. Additionally, Zhao et al. [49] indicated that the specified coating exhibited a lifetime of only 166 cycles during a thermal cycling test (with heating at 1100°C for 30 minutes per cycle). These results serve as evidence that NiCrBSi (BC) and WC (TC) enhanced composites used as coatings demonstrate sufficient thermal resistance and service life, primarily due to the greater compatibility of metal matrix composites (MMCs) reinforced with a solid WC layer compared to ceramic coatings [50-53].

Table 7 Results of the thermal cycling test of this work are compared with previous studies.

Temp./time	Cycle/ hr	Thick. μm	Cooling	Coating/ Method	Ref.
1100 °C /30 min	600	300	Water	Ni-WC/FTHS	Present
1070°C/ 3 min	120	100BC/ 450 TC	Water	Ceramic/APS	[1]
1100°C/ 10 min	450	230TC/ 100 BC	Water	7YSZ/ PS	[46]
1100°C /30 min	166	750TC/ 135 BC	Water	8YSZ/ PS	[49]

4. CONCLUSIONS

The chemical, morphological, microstructural, mechanical and thermal properties of samples coated with two coating layers were studied, the first was a bond coat (BC) made of (NiCrBSi) powder and the second was Ni-WC as a top coat (TC) sprayed on an IN718 substrate using thermal flame spraying, and spray conditions selected by the Taguchi method, and the following conclusions were reached:

- A coating with a thickness, 200-300 μm was successfully deposited using the FTHS method.
- The optimum FTHS parameters were selected according to the Taguchi method. They were as follows: SOD (150 mm), FR (30 g/min), and TV (300 mm/min). The most influential parameter in the spraying process was SOD, followed by FR, then TV.
- Based on optical microscope, scanning electron microscope (SEM), and EDS tests of the surface and cross-section, it was found that the coating layers consist of a spherical nano-microparticle structure with sizes ranging from 300 nm to 1.6μm. This confirms the process of dissolving most of the coating particles and depositing them on the samples as a layer free of cracks and with minimal porosity. X- ray diffraction (XRD) also indicated that the coating mainly consisted of crystalline and non-crystalline structures of γ-Ni, carbides, borides, and metal compounds. The phases were evenly spread throughout the coating.
- Microhardness results indicated that the hardness of the coated samples increased by more than four times when comparing the samples before and after coating. This enhancement is attributed to the presence of hard ceramic particles, such as tungsten carbide (WC), within the nickel-based matrix coating.
- The thermal cycling test indicated that the highest thermal shock resistance was obtained with a 300μm coating. This improvement is attributed to the role of the coating layer, which consists of γ-Ni, carbides such as WC and Cr7C3, borides like CrB, and metal compounds such as Ni3Si work together to reduce the formation of a harmful oxide layer.

In this research, it was found that the application of NiCrBSi as a bonding layer and Ni-WC as a composite top layer on Inconel 718 superalloy substrate via FTHS technique was successful, forming a protective layer with a cohesive and dense microstructure with negligible porosity, adhesion and high hardness, designed to perform efficiently against thermal shock effects at high temperatures.

References

[1] E. Poursaeidi, K. Torkashvand, M. Mohammadi, International Journal of Engineering (IJE), Transactions C: Aspects, 32 (2019) 872. https://doi.org/10.5829/ije.2019.32.06c.11
[2] J. Aust, D. Pons, Aerospace, 6 (2019) 58. https://doi.org/10.3390/aerospace6050058
[3] Y.-F. Hsiao, Y.-C. Shiah, Aerospace, 10 (2023) 885. https://doi.org/10.3390/aerospace10100885
[4] T. Saidani, M. Zaabat, M. S. Aida, R. Barillé, M. Rasheed, Y. Almohamed, Journal of Materials Science: Materials in Electronics, 28 (2017) 9252. https://doi.org/10.1007/s10854-017-6660-9

[5] M. Tahari, F. Naeimi, International Journal of Engineering (IJE), Transactions C: Aspects, 30 (2017) 433. https://doi.org/10.5829/idosi.ije.2017.30.03c.13
[6] R. A. Anaee, M. A. Abbas, S. A. Abdul Maged, S. A. Naser, S. S. Hamdi, H. M. Yousif, N. J. Al-Bahnam, T. A. Anai, Experimental and Theoretical NANOTECHNOLOGY, 9 (2025) 449. https://doi.org/10.56053/9.S.449
[7] E. T. Abdullah, M. R. Khasheet, Z. N. Hasheem, Experimental and Theoretical NANOTECHNOLOGY, 9 (2025) 347. https://doi.org/10.56053/9.2.347
[8] M. Sulaiman, E. M. Hadi, Experimental and Theoretical NANOTECHNOLOGY, 9 (2025) 431. https://doi.org/10.56053/9.S.431
[9] A. J. Hussein, M. N. Al-Darraji, M. Rasheed, IOP Conference Series: Earth and Environmental Science, 1262 (2023) 022007. https://doi.org/10.1088/1755-1315/1262/2/022007
[10] M. B. Toparli, F. Sen, O. Çulha, E. Çelik, Journal of Materials Processing Technology, 190 (2007) 26. https://doi.org/10.1016/j.jmatprotec.2007.03.115
[11] A. S. Praveen, J. Sarangan, S. Suresh, B. H. Channabasappa, Ceramics International (2024). (Please verify the DOI—the DOI in your list corresponds to a 2015 paper and appears inconsistent.)
[12] E. Kadri, M. Krichen, R. Mohammed, A. Zouari, K. Khirouni, Optical and Quantum Electronics, 48 (2016) 1. https://doi.org/10.1007/s11082-016-0812-7
[13] M. Rahnavard, A. G. Ostad, International Journal of Engineering (IJE), Transactions A: Basics, 30 (2017) 101. https://doi.org/10.5829/idosi.ije.2017.30.01a.13
[14] S. S. Batros, M. Rasheed, H. K. Aity, A. A. Hatef, T. Saidani, Materials Chemistry and Physics, 355 (2026) 132243. https://doi.org/10.1016/j.matchemphys.2026.132243
[15] B. A. Ahmed, M. Hussain, H. M. Yousif, AIP Conference Proceedings, 3051 (2024). https://doi.org/10.1063/5.0191738
[16] M. Mudhafar, Z. Shihab, H. Al-, Acta Physica Polonica A, 134 (2018) 248. https://doi.org/10.12693/APhysPolA.134.248
[17] M. Bober, J. Jakubowski, A. Radziszewski, J. Senkara, Advances in Materials Science, 18 (2018) 24. https://doi.org/10.1515/adms-2017-0047
[18] A. Günen, A. Çürük, JOM, 72 (2020) 673. https://doi.org/10.1007/s11837-019-03950-6
[19] M. Rasheed, A. Khaleefah, Materials Chemistry and Physics, 355 (2026) 132112. https://doi.org/10.1016/j.matchemphys.2026.132112
[20] R. Rachida, B. El K., F. D., V. V., D. Dorian, Journal of Materials and Environmental Science, 8 (2017) 4550. https://doi.org/10.26872/jmes.2017.8.12.480
[21] T. Rashid, M. M. Mokji, M. Rasheed, Journal of the Mechanical Behavior of Materials, 34 (2025) 1. https://doi.org/10.1515/jmbm-2025-0074
[22] S. Joshi, P. Nylen, Technologies, 7 (2019) 79. https://doi.org/10.3390/technologies7040079
[23] P. Senapati, H. Sutar, R. Murmu, S. Bajpai, Journal of Composites Science, 5 (2021) 133. https://doi.org/10.3390/jcs5050133
[24] D. Frunzaverde, G. Marginean, C. R. Ciubotariu, Crystals, 14 (2024) 1078. https://doi.org/10.3390/cryst14121078
[25] M. Rasheed, I. Alshalal, A. A. Rashed, M. A. Sarhan, A. S. Jaber, Indonesian Journal of Electrical Engineering and Computer Science, 33 (2024) 653. https://doi.org/10.11591/ijeecs.v33.i1.pp653-660
[26] N. Aya, M. Hussain, S. Sura, Advances in Mechanics, 9 (2021) 853. https://doi.org/10.13140/RG.2.2.11690.34246
[27] M. M. Mihoob, H. G. Mohammed, T. M. B. Albarody, F. Ahmad, M. S. Alnarabiji, Energies, 15 (2022) 9415. https://doi.org/10.3390/en15249415
[28] M. Rasheed, M. N. Mohammedali, F. A. Sadiq, M. A. Sarhan, T. Saidani, Journal of Optics, 54 (2024) 1. https://doi.org/10.1007/s12596-024-01928-5

[29] G. Singh, M. Kaur, R. Upadhyaya, Journal of Thermal Spray Technology, 28 (2019) 1081. https://doi.org/10.1007/s11666-019-00876-y
[30] A. A. Hateef, E. Dhahri, M. Rasheed, H. Kadhim, Z. Abbas, N. Hassan, Physics and Chemistry of Solid State, 25 (2024) 801. https://doi.org/10.15330/pcss.25.4.801-810
[31] K. Yuan, Y. Yu, J.-F. Wen, Vacuum, 137 (2017) 72. https://doi.org/10.1016/j.vacuum.2016.12.033
[32] I. M. Mohammed, M. Rasheed, AIP Conference Proceedings, 3321 (2025) 020026. https://doi.org/10.1063/5.0289719
[33] G. Prasanna, S. Prasanta, Procedia Engineering, 97 (2014) 439. https://doi.org/10.1016/j.proeng.2014.12.268
[34] R. S. Mahmood, et al., Journal of the Mechanical Behavior of Materials, 34 (2025) 1. https://doi.org/10.1515/jmbm-2025-0040
[35] Z. Bergant, J. Grum, Journal of Thermal Spray Technology, 18 (2009) 380. https://doi.org/10.1007/s11666-009-9304-7
[36] F. Gao, X. Huang, R. Liu, et al., Journal of Thermal Spray Technology, 21 (2012) 176. https://doi.org/10.1007/s11666-011-9700-7
[37] F. Boudou, A. Guendouzi, A. Belakredar, M. RASHEED, Notulae Scientia Biologicae, 16 (2024) 13837. https://doi.org/10.55779/nsb16211837
[38] A. Keziz, M. Rasheed, M. Heraiz, F. Sahnoune, A. Latif, Ceramics International, 49 (2023) 37423. https://doi.org/10.1016/j.ceramint.2023.09.068
[39] J T. Rashid, M. M. Mokji, M. Rasheed, Journal of Optics, 53 (2024) 1. https://doi.org/10.1007/s12596-024-02080-w
[40] F. Boudou, A. Belakredar, A. Berkane, M. RASHEED, Notulae Scientia Biologicae, 17 (2025) 12183. https://doi.org/10.55779/nsb17212183
[41] R. Fleischer, D. Dimiduk, H. Lipsitt, Annual Review of Materials Science, 19 (1989) 231. https://doi.org/10.1146/annurev.ms.19.080189.001311
[42] J. J. Ruan, N. Ueshima, K. Oikawa, Journal of Alloys and Compounds, 814 (2020) 152289. https://doi.org/10.1016/j.jallcom.2019.152289
[43] Z. Bergant, B. Š. Batič, I. Felde, R. Šturm, M. Sedlaček, Materials, 15 (2022) 342. https://doi.org/10.3390/ma15010342
[44] M. Shi, Z. Xue, Z. Zhang, X. Ji, E. Byon, S. Zhang, Surface and Coatings Technology, 395 (2020) 125913. https://doi.org/10.1016/j.surfcoat.2020.125913
[45] M. S. Ibrahim, T. T. Issa, B. Yaqoob, E. N. Fayyadh, A. Rashid, R. S. Mahmood, Experimental and Theoretical NANOTECHNOLOGY, 10 (2026) 887. https://doi.org/10.56053/10.S.887
[46] H. M. I. Al-Zuhairi, I. Alshalal, H. H. Abbood, M. Al Nuaimi, Experimental and Theoretical NANOTECHNOLOGY, 10 (2026) 855. https://doi.org/10.56053/10.S.855
[47] H. M. I. Al-Zuhairi, I. Alshalal, H. H. Abbood, M. Al Nuaimi, Experimental and Theoretical NANOTECHNOLOGY, 10 (2026) 1093. https://doi.org/10.56053/10.S.1093
[48] F. Boudou, A. E. Sabar, M. I. Majeed, A. M. Ibraham, R. Jamal, A. Rashid, A. Belakredar, M. Bendahmane-Salmi, M. RASHEED, R. RASHEED, T. Saidani, H. D. Al-Bahadli, Experimental and Theoretical NANOTECHNOLOGY, 10 (2026) 821. https://doi.org/10.56053/10.S.821
[49] A. R. J. Katae, H. H. Hussein, A. S. Jaber, M. A. Sarhan, M. RASHEED, Experimental and Theoretical NANOTECHNOLOGY, 10 (2026) 725. https://doi.org/10.56053/10.2.725
[50] G. E. Alkinani, A. R. J. Katae, M. RASHEED, Experimental and Theoretical NANOTECHNOLOGY, 10 (2026) 1027. https://doi.org/10.56053/10.S.1027
[51] A. Ashofteh, et al., Ceramics–Silikáty, 62 (2018) 200. https://doi.org/10.13168/cs.2018.0013
[52] O. Alabdali, A. Guessab, Filomat, 34 (2020) 601. https://doi.org/10.2298/FIL2002601A

[53] O. Y. M. Alabdali, A. Guessab, Applied Mathematics and Computation, 247 (2014) 1129. https://doi.org/10.1016/j.amc.2014.09.00